Journal of Ceramic Processing Research. Vol. 15, No. 6, pp. 382~388 (2014)

J O U R N A L O F
Ceramic Processing Research

Homogeneous precipitation synthesis and photoluminescence properties of $La_2O_2SO_4 : Eu^{3+}$ quasi-spherical phosphors

Jingbao Lian*, Ping Liang, Bingxin Wang and Feng Liu
School of Mechanical Engineering, Liaoning Shihua University, Fushun, 113001, P.R.China

Synthesis and photoluminescence properties of $La_2O_2SO_4 : Eu^{3+}$ quasi-spherical phosphors were investigated by homogeneous precipitation from $La(NO_3)_3$, $Eu(NO_3)_3$, $(NH_4)_2SO_4$ and urea ($(CO(NH_2)_2$) as the starting materials. It was found that the yield of the precursor is strongly dependent on *m* value, namely, the molar ratio of urea to $La(NO_3)_3$, and the optimal *m* value is 10. Thermal analysis, FT-IR and XRD show the optimal precursor is composed of $La_2(OH)_2CO_3SO_4 \cdot 2H_2O$ and can be converted into pure $La_2O_2SO_4$ phase at a temperature higher than 600 °C for 1 h in air. SEM observation shows that the obtained $La_2O_2SO_4$ phosphor particles are quasi-spherical in shape and narrow distribution with a mean particle size of about 2 μm. Photoluminescence spectra reveal that the emission intensities of the $La_2O_2SO_4 : Eu^{3+}$ phosphors depend on the calcination temperature and the strongest emission peak is located at 620 nm under 280 nm UV light excitation for the $La_2O_2SO_4 : Eu^{3+}$ phosphors calcined at 1000 °C, which corresponds to the $^5D_0 \rightarrow {}^7F_2$ transition of Eu^{3+} ions. The quenching concentration of Eu^{3+} ions is 5 mol% and the concentration quenching mechanism is the electric dipole-quadrupole interaction for the $^5D_0 \rightarrow {}^7F_2$ transition of Eu^{3+} ions.

Key words: Luminescent materials, Rare earth oxysulfate, Homogeneous precipitation synthesis, Photoluminescence.

Introduction

Considerable interests have been focused on rare earth oxysulfate compounds (general formula $Ln_2O_2SO_4$) due to their significant physical properties. For $Ln_2O_2SO_4$, the earlier works focused on the magnetic properties of $Gd_2O_2SO_4$ at low temperatures [1-2]. In addition, it is noteworthy that rare earth ions doped $Ln_2O_2SO_4 : Re^{3+}$ (Ln = La,Y,Gd; Re = Ce, Eu, Tb) materials may also display unique luminescent behaviors [3-10]. Lanthanum oxysulfate ($La_2O_2SO_4$) belongs to the family of $Ln_2O_2SO_4$ compounds and the research of $La_2O_2SO_4$ mainly focuses on oxygen storage-release properties [11-15] and solid electrolyte [16] for the moment. Moreover, the crystal structure of $La_2O_2SO_4$ is usually the alternative stacking of a $La_2O_2^{2+}$ layer and a layer of sulfate (SO_4^{2-}), and that of La_2O_2S is the alternative stacking of a $La_2O_2^{2+}$ layer and a layer of sulfide (S^{2-}) [17]. Thus, $La_2O_2SO_4$ is an intermediate phase for the synthesis of lanthanum oxysulfide (La_2O_2S), and is usually used as a precursor for the synthesis of La_2O_2S in reduction atmosphere.

Generally speaking, $La_2O_2SO_4$ is an intermediate phase during the thermal decomposition of hydrated lanthanum sulfate ($La_2(SO_4)_3 \cdot 8H_2O$), thus it can be synthesized by heating commercial $La_2(SO_4)_3 \cdot 8H_2O$ at 900 C for 5 h in a flowing N_2 or air atmosphere [12, 18-19]. Moreover, $La_2O_2SO_4$ can be aslo prepared by heating La_2S_3 at 1000 °C for 12 h in air [16]. However, the above mentioned methods are a high temperature, time-consuming preparation process and realeasing of sulfur oxide (SO_2 or SO_3) is harmful to the environment. Homogeneous precipitation synthesis is one of the most promising techniques because of its advantages such as the relatively simple synthetic route, low cost, ease of mass production, and so on. In this study, we proposed a homogeneous precipitation to synthesize $La_2O_2SO_4 : Eu^{3+}$ quasi-spherical phosphors using $La(NO_3)_3$, $Eu(NO_3)_3$, $(NH_4)_2SO_4$ and urea as the starting materials and investigated their photoluminescence properties.

Experimental

$La(NO_3)_3 \cdot 6H_2O$ (AR), $Eu(NO_3)_3 \cdot 6H_2O$ (AR), $(NH_4)_2SO_4$ (AR) and urea (AR) were used as the starting materials. All reagents were purchased from Sinopharm Chemical Reagent Co. Ltd, China. Firstly, the $La(NO_3)_3$ solution (0.1 M) was obtained by dissolving a stoichiometric amount of $La(NO_3)_3 \cdot 6H_2O$ in deionized water followed by adding $(NH_4)_2SO_4$ and urea to form mother liquor with molar ratio of 2 : 1 : *m* for $La^{3+} : SO_4^{2-}$: urea. Here, *m* value was set at 2.5, 5, 7.5 and 10, respectively. Next, the mother liquor was heated at 80 °C for 2 h in a water bath. The resulted white precipitations were separated centrifugally, washed several times with deionized water and dried at

*Corresponding author:
Tel : +86-24-56865042
Fax: +86-24-56865042
E-mail: lianjingbao@aliyun.com

80 °C for 8 h to obtain the precursors. Finally, the precursors were dried at 80 °C and calcined at different temperatures for 1 h in air to form target products. Furthermore, trivalent europium (Eu^{3+}) doped $La_2O_2SO_4$ phosphors were also obtained by similar process. The concentration of Eu^{3+} ions was set in the range of 2.5 mol% ~ 15 mol% and was compensated by an equivalent decrease of La^{3+} ions.

Thermal analysis, i.e. thermogravimetry (TG), derivative thermogravimetry (DTG) and differential thermal analysis (DTA), was performed using simultaneous differential thermal analysis and thermo-gravimetry (SDT 2960) with 5 °C · min^{-1} heating rate in the air. Fourier transform infrared spectra (FT-IR) were recorded in the region of 4000 ~ 400 cm^{-1} using a Perkin-Elmer FT-IR spectrophotometer by the KBr method. Phase analysis of the synthesized products were identified by X-ray diffractometer (XRD, SHIMADZU-7000) operating at 40 kV and 30 mA, using Cu Kα (1.5406 Å) radiation. The particle morphology of the synthesized products were observed by a VEGA3 TESCAN scanning electron microscope (SEM). Photoluminescence (PL) spectra of the $La_2O_2SO_4:Eu^{3+}$ phosphors were obtained on a Perkin-Elmer LS55 fluorescent spectrophotometer equipped with a 150 W xenon lamp as the excitation source. All measurements were performed at room temperature.

Results and Discussion

Formation mechanism and selection of *m* value

In this study, the hydrolyzation process of $La(NO_3)_3$ can provide La^{3+} ions. $(NH_4)_2SO_4$ undergoes hydrolysis and liberates SO_4^{2-} groups. Moreover, urea is a weak brönsted base and releases a certain quantity of CO_3^{2-} and OH groups in the present heating condition. According to hard-soft acid-base principle (HSAB), hard acids prefer to bind to hard bases and soft acids prefer to bind to soft bases [20]. In the present reaction system, SO_4^{2-}, CO_3^{2-} and OH groups are hard bases and the hardness has the following order: $SO_4^{2-} > CO_3^{2-} > OH$, La^{3+} ions are hard acids. Then it is not difficult to bond each other to form lanthanum hydroxyl, carbonate and sulfate. The chemical reactions in the formation of the precursor can be expressed as follows:

$$La(NO_3)_3 \Leftrightarrow La^{3+} + 3NO_3^- \quad (1)$$

$$(NH_4)_2SO_4 \Leftrightarrow NH_4^+ + SO_4^{2-} \quad (2)$$

$$CO(NH_2)_2 + 4H_2O \Leftrightarrow 2NH_4OH + H_2CO_3 \quad (3)$$

$$NH_4OH \Leftrightarrow NH_4^+ + OH^- \quad (4)$$

$$H_2CO_3 \Leftrightarrow 2H^+ + CO_3^{2-} \quad (5)$$

$$2La^{3+} + 2m\alpha OH^- + m\alpha CO_3^{2-} + SO_4^{2-} + xH_2O \Leftrightarrow La_2(OH)_{2m\alpha}(CO_3)_{m\alpha}(SO_4)\cdot xH_2O \quad (6)$$

In the above Eqs.(6), α is the degree of dissociation for urea hydrolysis ($\alpha << 1$). From Eqs.(6), at the precipitation equilibrium

$$K\alpha = [La^{3+}]^2[OH^-]^{2m\alpha}[CO_3^{2-}]^{m\alpha}[SO_4^{2-}] \quad (7)$$

At a certain temperature, K*a* (equilibrium constant) is a constant. As $[La^{3+}]$ and $[SO_4^{2-}]$ were fixed in this study, $[OH^-]$ and $[CO_3^{2-}]$ were the factors affecting precipitation. As *m* value is increased, equation (7) can be satisfied more easily. In order to precipitate the La^{3+}

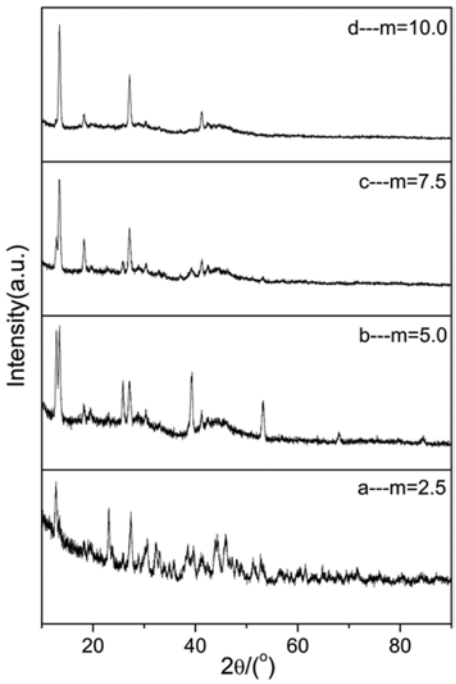

Fig. 1. XRD patterns of the precursors with different m values.

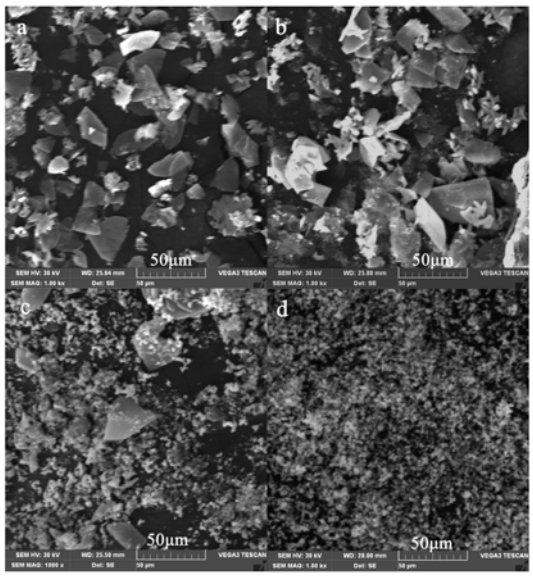

Fig. 2. SEM images of the precursor with different m values.

ions completely, appropriate *m* value should be selected. The effect of *m* value on the crystallinity and phase composition was investigated by XRD for all the precursors, as shown in Fig. 1. All the precursors are crystalline state in structure with obvious diffraction peaks. By increasing *m* value from 2.5 to 10, more sharp diffraction peaks appeared in the XRD patterns. However, the obtained diffraction pattern is inconsistent with the data reported in JCPD card database and the crystal structure are yet to be unidentified, which may attribute to the formation of a new $La_2(OH)_2CO_3SO_4 \cdot 2H_2O$ phase containing OH^-, CO_3^{2-} and SO_4^{2-} groups. This is confirmed by FT-IR spectroscopy and DTA-TG-DTG analysis in the following section.

The effect of *m* value on the morphologies was also examined by SEM for all the precursors. Fig. 2 presents the SEM images of the precursors with different *m* value. It is noted that *m* value is the key factor for the morphological features of the precursors. When $m = 2.5$ or 5, it can be clearly seen from Fig. 2a and Fig. 2b that the precursor particles are mostly the polyhedral in shape and about 20 ~ 30 μm in size. By increasing *m* value to 7.5, shown in Fig. 2c, the precursor particles are predominantly quasi-spherical morphologies with about 2 μm in diameter and partly the polyhedral shape with length of 30 μm in size. However, when $m = 10$, no polyhedral particles can be observed from Fig. 2d, the obtained precursor particles consist of weak agglomerates, which are formed by the interconnection of quasi-spherical particles. The particles is found to be about 2 μm in diameter and narrow distribution. The above investigation might be explained as follows. In this study, the OH^- and CO_3^{2-} concentration in solution increase with increasing *m* value. This, in turn, leads to the increasing supersaturation. According to the Gibbs-Thomson formula of classical nucleation theory [21]:

$$J = A\exp[-B(\ln S)^{-2}] \quad (8)$$

where J and S are nucleation rate and supersaturation, A and B are constants, respectively. Accordingly, the nucleation rate shows the increment tendency with increasing *m* value. Under low nucleation rate condition, the nucleus growth will not be subjected to limitation and the free growth of crystal faces will take place, leading to the formation of polyhedral particle. However, when *m* value is high enough (i.e. $m = 10$), the nucleation speeds up and the nucleus number increases significantly. Thus, the growth is restricted in the limited reaction volume by higher nucleus number, resulting in the formation of small spherical particles. In addition, the yield of precipitate aslo showed the increment tendency with increasing *m* value. Therefore, the $m = 10$ was selected as the optimal value for synthesizing the precursor in the follwing section.

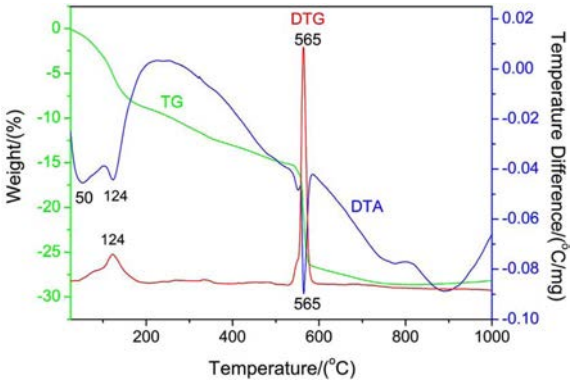

Fig. 3. Thermoanalytical (DTA,TG and DTG) curves of the optimal precursor in air.

Transformations of the optimal precursor during calcining

To understand the decomposition behaviors and determine the calcination temperature for the precursor, DTA-TG-DTG of the optimal precursor was conducted from room temperature to 1000 ºC and the results are shown in Fig. 3. The TG curve shows a continuous weight loss between room temperature and 1000 ºC with an overall weight loss of approximately 28.16 wt%. The total weight loss mainly consists of the following steps in the whole temperature range, as seen from the DTG curve. The weight loss in the temperature range from room temperature to ~ 150 ºC is about 7.34 wt%, which seems to be related mostly to removal of physically adsorbed water from the precursor. This weight loss corresponds to two weak endothermic peaks at around 50 ºC and 124 ºC in the DTA curve, and DTG maxima at about 124 ºC in the DTG curve. The weight loss between ~ 150 ºC and ~ 500 ºC is about 7.41 wt% (theoretical weight loss: 7.14 wt%), and no obvious endothermic peak in the DTA curve, which proceeds according to the following reaction:

$$La_2(OH)_2CO_3SO_4 \cdot 2H_2O = La_2(OH)_2CO_3SO_4 + 2H_2O\uparrow \quad (9)$$

The weight loss in the temperature range from ~ 500 ºC to ~561.5 ºC is about 3.75 wt% (theoretical weight loss: 3.85 wt%), which is associated with the complete dehydroxylation of the precursor with a weak endothermic peak at around 550 ºC in the DTA curve. This weight loss corresponds to the following reaction:

$$La_2(OH)_2CO_3SO_4 = La_2OCO_3SO_4 + H_2O\uparrow \quad (10)$$

The last weight loss of about 9.62 wt % starting at ~ 550 ºC (theoretical weight loss: 9.78 wt%) is associated with the complete decomposition of CO_3^{2-} anions of the precursor according to the following

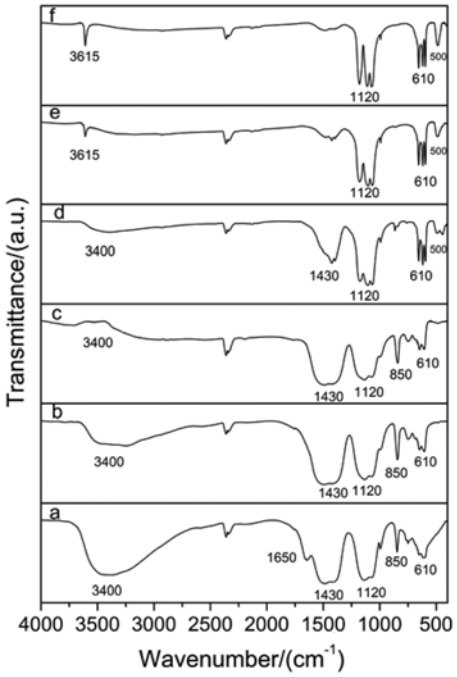

Fig. 4. FT-IR spectra of the precursor and its calcination products at different temperatures.

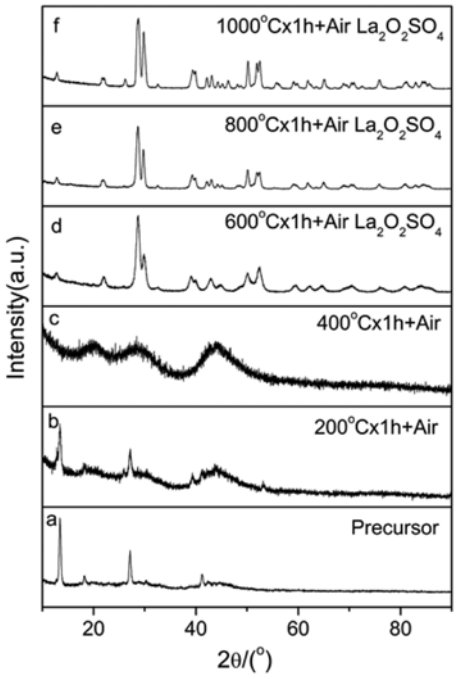

Fig. 5. XRD patterns of the precursor and its calcination products at different temperatures.

reaction:

$$La_2OCO_3SO_4 = La_2O_2SO_4 + CO_2\uparrow \quad (11)$$

At the same time, this weight loss accompanies with an obvious endothermic peak at around 565 ºC in the DTA curve, and a strong peak at about 565 ºC in the DTG curve. Moreover, as shown in Fig. 3, little weight changes can be observed at temperatures greater than 600 ºC on the TG curve, which indicates that at higher than 600 ºC the thermal decomposition is basically finished in the present study.

FT-IR analysis was performed to gain more insight into the structure and composition of the synthesized products. Fig. 4 shows FT-IR spectra of the precursor and its calcined products at different temperatures, respectively. Evidence of the presence of hydroxyl (OH^-), carbonate (CO_3^{2-}) and sulfate (SO_4^{2-}) groups in the precursor can be obtained from FT-IR spectroscopy (Fig. 4a). The spectrum shows the absorption peaks of physically absorbed water, crystal water, hydroxyl groups [22] (near 3400 cm^{-1} and 1650 cm^{-1}), the CO_3^{2-} (near 1430 cm^{-1} and 850 cm^{-1}) and the SO_4^{2-} anions (near 1120 cm^{-1} and 610 cm^{-1}), which indicates that the precursor is composed of lanthanum hydroxyl, carbonate and sulfate groups with some crystal water. After the precursor calcinined at 200 ºC, the strong broad absorption band centered at 3400 cm^{-1} becomes weaker, and the peak centered at 1650 cm^{-1} disappears (Fig. 4b), suggesting the evaporation of physically adsorbed water from the precursor. With increasing calcination temperature to 400 ºC (Fig. 4c), the broad absorption band centered at 3400 cm^{-1} becomes negligible, indicating that the removal of crystal water from the precursor. No significant changes appear for other absorption peaks. With increasing calcination temperature to 600 ºC (Fig. 4d), the absorption band centered at 3400 cm^{-1} becomes negligible, which is associated with the dehydroxylation of hydroxyl groups in the precursor. The SO_4^{2-} absorption bands (~ 1120 cm^{-1}, and ~ 610 cm^{-1}) split into some narrow sharp peaks, the CO_3^{2-} absorption bands become weaker, and a new absorption peak centered about 500 cm^{-1} appears, which corresponds to the characteristic vibration peaks of La-O bond in the synthesized product. After the precursor calcinined at 800 ºC and 1000 ºC (Fig. 4e and Fig. 4f), a narrow absorption peak centered about 3615 cm^{-1} appears, the CO_3^{2-} absorption band (1430 cm^{-1}) become negligible, suggesting the decomposition of CO_3^{2-} anions in the precursor. The broad SO_4^{2-} absorption bands (1120 cm^{-1} and 610 cm^{-1}) split into some narrow peaks and the broad La-O bond peak (500 cm^{-1}) still exist, indicating that the precursor has been gradually transform into $La_2O_2SO_4$ phosphor. These results are consistent with those obtained by the DTA-TG-DTG.

Fig. 5 shows the XRD patterns of the precursor and its calcined products at different temperatures, respectively. XRD analysis shows that the precursor is crystalline state in structure with essentially diffraction peaks, as shown in Fig. 5a. After the precursor calcinined at 200 ºC and 400 ºC (Fig. 5b and Fig. 5c), the XRD patterns show that the diffraction peaks become weak signal and gradually broaden, which corresponds to destruction of crystalline structure due

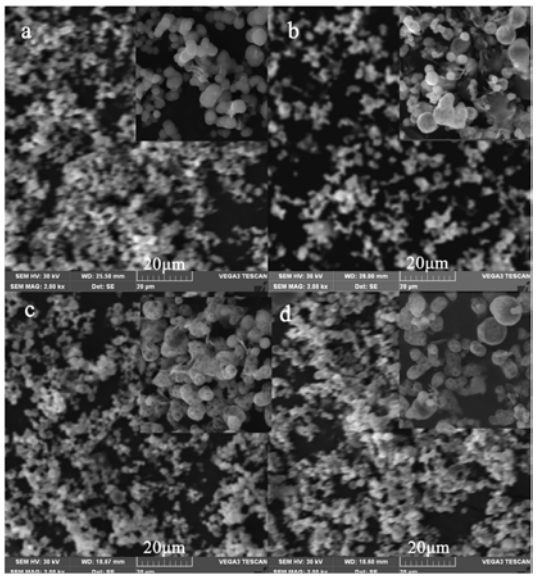

Fig. 6. SEM images of the precursor and its calcination products at different temperatures.

to removal of physically adsorbed water and crystal water. When the precursor was calcined at 600 °C, the diffraction peaks of pure $La_2O_2SO_4$ phase begin to appear in the XRD patterns (Fig. 5d) and the obtained diffraction patterns are well consistent with the data reported in JCPD card No. 00-016-0501. Further increase in the calcination temperature from 800 °C to 1000 °C leads to the enhanced $La_2O_2SO_4$ diffraction peak intensity because of the improvement of crystallinity (Fig. 5e and Fig. 5f). These results are also consistent with those obtained by using the DTA-TG-DTG analysis and the FT-IR spectra.

Fig. 6 shows the SEM images of the precursor and its calcined products at various temperatures, respectively. It can be seen from Fig. 6a that the precursor particles are quasi-spherical in shape, narrow distribution and about 2 μm in size. The surface of phosphor particles are smooth. Compared to its precursor, as shown in Fig. 6b- Fig. 6d, the resultant posphors, at any calcination temperature, show similar morphology to that of the precursor, which are still quasi-spherical shape and narrow distribution. However, the average particle size increased slightly with the increasing calcination temperature. Moreover, it is interesting to note that the particles are porous spheres and the particle surfaces are coarse. The reason for which is probably the evolution of H_2O and CO_2 gases due to thermal decomposition of the precursor during calcination.

PL spectra of the $La_2O_2SO_4 : Eu^{3+}$ phosphors

Excitation spectra of the $La_2O_2SO_4$:Eu^{3+} phosphors were taken by monitoring the wavelength of 620 nm. Since all the $La_2O_2SO_4 : Eu^{3+}$ phosphors have similar profiles of excitation and emission spectra, the spectra of $(La_{0.95,}\ Eu_{0.05})_2O_2SO_4$ were selected as an example. Fig. 7 shows the excitation and emission spectra of the $(La_{0.95,}\ Eu_{0.05})_2O_2SO_4$ phosphors calcined at different temperatures. It can be seen from Fig. 7 that the excitation and emission intensitie of the composed bands depend on the calcination temperature. With increasing calcination temperature, the main luminescence peak intensity increases significantly because of the improvement of crystallinity and the elimination of defects. As can be seen from Fig. 7a, a broad absorption band with a maximum at 280 nm exists, which is resulted from the charge-transfer (CT) transitions between O^2, S^2 and Eu^{3+} ions. The weak narrow peaks in the near UV range of the excitation spectrum are assigned to intra-configurational *4f-4f* transitions of Eu^{3+} ions in the oxysulfate host lattices, and the peaks at 395 nm and 465 nm are attributed to the $^7F_0 \rightarrow {}^5L_6$ and $^7F_0 \rightarrow {}^5D_2$ transitions of Eu^{3+} ions. In addition, the intra-configurational $4f^6$ excitation lines of the Eu^{3+} ions are very weak, indicating that the excitation of Eu^{3+} ions through the CT state for emission would be very efficient. The emission spectrum of $(La_{0.95,}\ Eu_{0.05})_2O_2SO_4$ under 280 nm UV light excitation (Fig. 7b) demonstrates the well-known $^5D_0 \rightarrow {}^7F_j$ (j = 1, 2, 3, 4) transitions of Eu^{3+} ions. The strongest emission peak located at 620 nm corresponds to the forced electric dipole $^5D_0 \rightarrow {}^7F_2$ transition of Eu^{3+} ions. These are typical emission peaks of Eu^{3+} ions in an oxysulfate host and no peak appears at 626 nm (a typical emission peak in the La_2O_3 host), which further confirm the formation

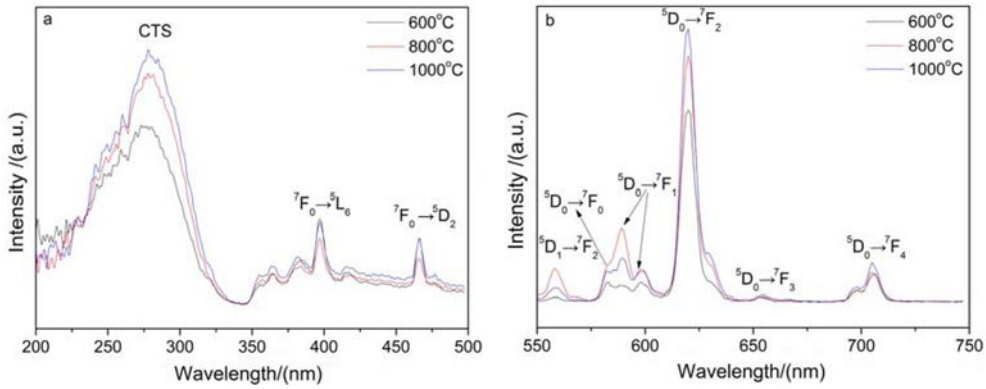

Fig. 7. Excitation (a) and emission spectra (b) of the $(La_{0.95}, Eu_{0.05})_2O_2SO_4$ phosphors calcined at different temperatures.

of pure $(La_{0.95,}\ Eu_{0.05})_2O_2SO_4$ phase. It is well known that the electric-dipole-allowed $^5D_0 \rightarrow {}^7F_2$ transition is hypersensitive to the local environment around Eu^{3+} ions and its intensity depends on the symmetry of the crystal field around Eu^{3+} ions. When Eu^{3+} ions is located at a low-symmetry local site (without an inversion center), this emission is often dominant in the emission spectrum. So the site in $(La_{1-x},\ Eu_x)_2O_2SO_4$ occupied by Eu^{3+} ions has no inversion symmetry. The emission peak at around 580 nm is assigned to the $^5D_0 \rightarrow {}^7F_0$ transition [7]. It is known that the $^5D_0 \rightarrow {}^7F_0$ transition is very sensitive to the local environment of Eu^{3+} ion. According to the parity selection rule, optical transition from the $^5D_0$ to $^7F_0$ levels are strictly forbidden if the Eu^{3+} ion occupies an inversion symmetry site in the crystal lattice. However, if the site occupied by Eu^{3+} ion has no inversion symmetry (Cs, C_n, or C_{nv}) symmetry, the uneven crystal field components can lead to the mixing of opposite parity states into the $4f^n$ configuration levels. In such a case, the $^5D_0 \rightarrow {}^7F_0$ transition becomes not strictly forbidden and thus gives rise to weak lines in the emission spectrum. In addition, the number of the $^5D_0 \rightarrow {}^7F_0$ transition equal to that of the lattice sites occupied by Eu^{3+} ion. The only one $^5D_0 \rightarrow {}^7F_0$ emission peak at 580 nm might then indicate that the Eu^{3+} ions in orthorhombic $(La_{1-x},\ Eu_x)_2O_2SO_4$ have Cs, C_n, or C_{nv} site symmetry [8]. The asymmetrically split emission peaks at 595 nm and 702 nm are assigned to the $^5D_0 \rightarrow {}^7F_1$ and the $^5D_0 \rightarrow {}^7F_4$ transitions of Eu^{3+} ions, respectively. The asymmetrically split emission peaks at 590 nm and 705 nm are assigned to the $^5D_0 \rightarrow {}^7F_1$ and the $^5D_0 \rightarrow {}^7F_4$ transitions of Eu^{3+} ions, respectively. The weak emission peak at 558 nm and the very weak emission peak at 654 nm are also observed, corresponding to $^5D_1 \rightarrow {}^7F_2$ and $^5D_0 \rightarrow {}^7F_3$ transitions, respectively. The photoluminescence intensity of a phosphor material is always dependent on dopant concentration. For the $La_2O_2SO_4:Eu^{3+}$ phosphors calcined at 1000 °C, the emission intensity of the $^5D_0 \rightarrow {}^7F_2$ transition with different concentrations of Eu^{3+} ions under 280 nm UV light excitation is shown in Fig. 8. With increasing concentration of Eu^{3+} ions, the emission intensity of the $^5D_0 \rightarrow {}^7F_2$ (620 nm) transition first increases, reaching a maximum value at x = 5 mol% and then decreases due to concentration quenching. According to the literature [23], the relationship between emission intensity, *I*, and dopant concentration, *C*, can be expressed as follows:

$$log(I/C) = (-s/d)logC + logf \quad (12)$$

where *s* is the index of electric multipole, variable *d* is the dimension of the sample, which would equal 3 if energy transfer among the Eu^{3+} ions inside the particles is considered, and *f* is independent of the dopant concentration. The values of *s* are 6, 8, and 10 for the

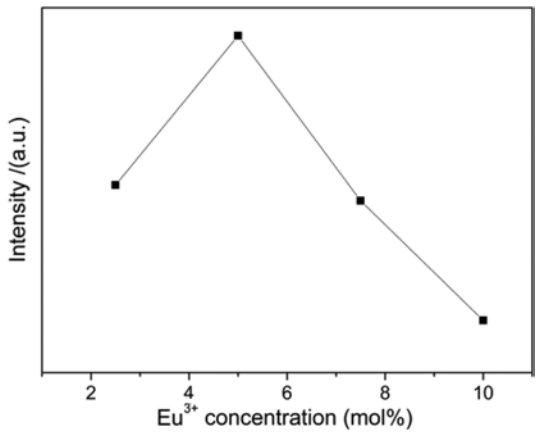

Fig. 8. The effects of Eu^{3+} concentration on PL intensity of the $(La_{1-x},Eu_x)_2O_2SO_4$ phosphors.

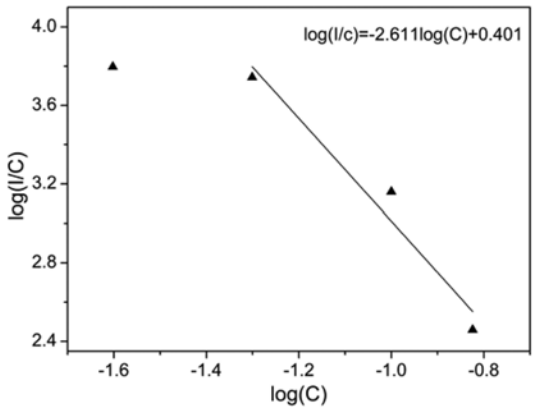

Fig. 9. The relationship between log (C) and log (I/C) for the $(La_{1-x},Eu_x)_2O_2SO_4$ phosphors.

electric dipole-dipole, electric dipole-quadrupole and electric quadrupole-quadrupole interactions, respectively. The variable $s = 3$ corresponds to the mechanism of exchange interaction. Fig. 9 shows the *log(I/C)-log(C)* plots for the $^5D_0 \rightarrow {}^7F_2$ transition of Eu^{3+} ions for the $La_2O_2SO_4:Eu^{3+}$ phosphors calcined at 1000 °C. According to equation (12) and using linear fittings to deal with the experimental data in the region of high concentrations, the slope parameter *–s/d* was determined to be –2.611 (close to –2.667), thus yielding an *s* value of 8. This indicates that the concentration quenching mechanism is the electric dipole-quadrupole interaction.

Conclusions

A homogeneous precipitation synthesis has been successfully developed for synthesizing pure $La_2O_2SO_4:Eu^{3+}$ quasi-spherical phosphors, which uses $La(NO_3)_3$, $Eu(NO_3)_3$, $(NH_4)_2SO_4$ and urea as the starting materials. The optimal precursor $(La_2(OH)_2CO_3SO_4 \cdot 2H_2O)$ can be transformed into pure $La_2O_2SO_4$ phosphor by calcining at higher than 600 °C for 1 h in air, which is largely quasi-spherical in shape, about 2 ~ 3 μm in diameter and narrow distribution. The

strongest emission peak for the $(La_{0.95,}Eu_{0.05})_2O_2SO_4$ phosphor calcined at 1000 °C was observed to be located at 620 nm under 280 nm UV light excitation. In sum, the results show that the homogeneous precipitation synthesis is a convenient and feasible method for synthesizing pure $La_2O_2SO_4 : Eu^{3+}$ red emitting phosphor.

Acknowledgments

This work is supported by the National Natural Science Foundation of China (51175240).

References

1. W. Paul, J. Magn. Magn. Mater. 87 (1990) 23-28.
2. W. Kratz, H.G. Kahle, W. Paul, J. Magn. Magn. Mater. 161 (1996) 249-254.
3. M. Shoji, K. Sakurai, J. Alloy. Comp. 426 (2006) 244-246.
4. A.M. Srivastava, A.A. Setlur, H.A. Comanzo, Y. Gao, M.E. Hannah, J.A. Hughes, U. Happek, Optical Materials 30 (2008) 1499-1503.
5. T. Kijima, T. Shinbori, M. Sekita, M. Uota, G. Sakai, J. Lumin. 128 (2008) 311-316.
6. T. Kijima, T. Isayama, M. Sekita, M. Uota, G. Sakai, J. Alloy. Comp. 485 (2009) 730-733.
7. P. Porcher, D.R. Svoronos, J. Solid State Chem. 46 (1983) 101-111.
8. J.B. Lian, X.D. Sun, Z.G. Liu, J.Y. Y, X.D. Li, Mater. Res. Bull. 44 (2009) 1822-1827.
9. J.B. Lian, X.D. Sun, X.D. Li, Mater. Chem. and Phys. 125 (2011) 479-484.
10. X.H. Liu, D. Zhang, J.H. Jiang, N. Zhang, R.Z. Ma, H.B. Zeng, B.P. Jia, S.B. Zhang, G.Z. Qiu RSC Advances, 2 (2012) 9362-9365.
11. D. Zhang, F. Yoshioka, K. Ikeue, M. Machida, Chem. Mater. 20 (2008) 6697-6703.
12. M. Machida, K. Kawamura, K. Ito, K. Ikeue, Chem. Mater. 17 (2005) 1487-1492.
13. M. Machida, K. Kawamura, K. Ito, Chem. Commun. 6 (2004) 662-663.
14. M. Machida, T. Kawano, M. Eto, D. Zhang, K. Ikeue, Chem. Mater. 19 (2007) 954-960.
15. K. Ikeue, T. Kawano, M. Eto, D. Zhang, M. Machida, J. Alloy. Comp. 451 (2008) 338-340.
16. S.Yamamoto, S. Tamura, N. Imanaka, J. Alloy. Comp. 418 (2006) 226-229.
17. S. Zhukov, A. Yatsenko, V. Chernyshev, V. Trunov, E. Tserkovnaya, O. Anston, Mater. Res. Bull. 32 (1997) 43-50.
18. L.C. Machado, M.T.D. de Azeredo, H.P.S. Corre^a, J.D.R. Matos, I.O. Mazali. J Therm Anal Calorim 107 (2012) 305-311.
19. E. I. Sal'nikova, D. I. Kaliev, P. O. Andreev. Russian J. Phys. Chem. A 85 (2011) 2121-2125.
20. L. H. Lee, Progr Colloid Polym Sci. 82 (1990) 337-344.
21. D.Y. Liu, S. Ren, G.S. Wang, L.S. Wen, J. Yu, J Mater Sci 44 (2009) 108-113.
22. G.X. Liu, G.Y. Hong, J.X. Wang, X.T. Dong, J. Alloy. Comp. 432 (2007) 200-204.
23. Q.L. Dai, H.W. Song, M.Y. Wang, X. Bai, B. Dong, R.F. Qin, X.S. Qu, H. Zhang. J. Phys. Chem. C. 112 (2008) 19399-19404.